Journal of Applied Fluid Mechanics, Vol. 5, No. 1, pp. 57-66, 2012.
Available online at www.jafmonline.net, ISSN 1735-3572, EISSN 1735-3645.
DOI: 10.36884/jafm.5.01.11958

Control of the Separation Flow in a Sudden Enlargement

A. Abdel-Fattah

Department of Mechanical Power Engineering, Faculty of Engineering Menoufyia University, Shebin El-Kom, Egypt.

†*Corresponding Author Email: ashourabdelfatah@yahoo.com*

(Received January 19, 2010; accepted August 4, 2010)

ABSTRACT

In the present paper, an experimental and numerical investigation of fluid flow and heat transfer in the case of wall injection besides main flow through a circular sudden enlargement are studied. The injected flow is achieved through an annular slot placed around the inner side wall of the step. The static pressure variation along the sudden enlargement length is measured and calculated at different values of injection ratio (Q) and injection flow angles. The average heat transfer with Reynolds number (Re_J) of injected flow at different values of the inlet flow angle is obtained. The velocity, turbulent kinetic energy and temperature contours are presented in this study. Reynolds number of injected flow is varied between 320 and 840, Reynolds number of main flow is between 5895 and 8450 and the injection flow angles are 0°, 15°, 30°, 45° and 60°. In the injection case, the results indicate that, the pressure recovery coefficient increases by decreasing the injection ratio and increasing the flow angle. The average heat transfer coefficient increases as both injection Reynolds number and the injection flow angle increase. The numerical results showed that two recirculation zones generate behind the step between the injection flow and the main flow. The size of these recirculation zones decreases by increasing the injection flow rate. The turbulent kinetic energy increases within region between the recirculation zones and main zone also, it decays by injecting flow in the recirculation zone. The length for higher value of flow temperature decreases by injecting flow in the recirculation zone, and that length increases as the injection flow rate increases. The comparison between the experimental results and the numerical results gives good agreement using the k-ε model with Leschziner and Rodi correction.

Keywords: Control flow, injection flow, separation flow, turbulent flow, heat transfer

NOMENCLATURE

A_f	cross sectional area of flow
A_s	surface area of heat transfer
c_1, c_2 , c_μ	empirical constants of k-ε model
Cp	pressure coefficient $\frac{\bar{p}-\bar{p}_{in}}{0.5\rho U_m^2}$
d_m	hydraulic parameter of the flow at inlet
d_i	inlet diameter of sudden enlargement, mm
d_n	inlet nominal diameter of sudden enlargement, mm
D_n	outlet nominal diameter of sudde enlargement, mm
h_{av}	average heat transfer coefficient, ($W.m^{-2}.K^{-1}$)
K	dimensionless of turbulent kinetic energy ($\bar{k}/U_m^2$)
k_c	thermal conductivity ($W.m^{-1}.K^{-1}$)
$\bar{k}$	turbulent kinetic energy ($J.kg^{-1}$)
P	dimensionless pressure
$\bar{p}$	static pressure ($N.m^{-2}$)
Pr	laminar Prandtl number
Pr_t	turbulent Prandtl number
Q	injection ratio ($\bar{Q}_J / \bar{Q}_m$)
Re_m	Reynolds number, $Re_m = \bar{\rho} U_m d_m / \mu$
Re_{mt}	turbulent Reynolds number, $Re_{mt} = \bar{\rho} U_m d_m / \bar{\mu}_t$
S_{ij}	deformation rate tensor
T	dimensionless temperature
$\bar{T}$	temperature (K)
U	dimensionless of axial component of local mean velocity, $u = \bar{u} / U_m$
$\bar{u}$	axial component of local mean velocity ($m.s^{-1}$)
U_j	injection mean velocity ($m.s^{-1}$)
U_m	inlet mean velocity of sudden Enlargement ($m.s^{-1}$)
v	dimensionless of radial component of local mean velocity, $v = \bar{v} / U_m$
$\bar{v}$	radial component of local mean velocity ($m.s^{-1}$)

r, z cylindrical coordinates

Greek Symbols

ε dimensionless of dissipation rate of k , $(\varepsilon = \bar{\varepsilon}\, d_m / U_m^3)$

$\bar{\varepsilon}$ dissipation rate of k ($J.kg^{-1}$)

μ dynamic viscosity ($kg.m^{-1}.s^{-1}$)

$\bar{\rho}$ density($Kg.m^{-3}$)

σ_ε model constant

σ_κ model constant

Subscripts

- dimension
av average
in inlet
j injection

1. INTRODUCTION

The mixing flow between injected annular flow and main flow inside the chamber are important for many engineering applications, for example fuel and air mixing in gas turbine engine combustor system. This flow is interesting in increasing the efficiency and performance of combustor chamber. A number of investigations had studied facing step flow. Yilmaz and Öztop (2006) studied numerically the turbulent forced heat transfer for double forward facing step flow. They used commercial FLUENT to illustrate the effect of step heights, step lengths and Reynolds numbers on the heat transfer and fluid flow. Their results showed that, the second step can be used as a control device for both heat transfer and fluid flow. A steady–state heat transfer for two dimensional laminar, incompressible, plane wall jet over a back ward –facing step was carried out by Kanna and Das (2006). They studied the effect of Reynolds number, Prandtl number and step geometry on the heat transfer characteristics. Their results indicated that, when Reynolds number increases, the isotherms are deflected toward the recirculation region and are concentrated near the wall. Also, when Reynolds number increases, local Nusselt numbers along the bottom wall increases to a peak value and is asymptotically reduced in the downstream direction. Seo and Parameswaran (2002) studied numerically the steady and unsteady flow through a back ward facing step. They used the standard k-ε model with standard wall functions to compute the buoyancy flow for various values of the Richardson number. Their results showed that, for the flow over the back ward- facing step, buoyancy –driven vortex shedding has been noticed only in the turbulent flow when Richardson number increases to the a critical value. The control of the isothermal turbulent flow within a rearward- facing step combustor using countercurrent shear was studied experimentally by Forliti and Strykowoski (2005). Their results indicated that the use of suction based counter flow has essentially to separate mechanisms for achieving shear flow control. First counter flow has an effect of increasing the natural reverse flow, caused by the sudden expansion of the step. The second mechanism employed using the counter flow is the modification of the shear layer near the expansion plane. Manca *et al.* (2003) studied numerically the effect of heated wall position on the mixed convection in a channel with an open cavity. Their results are reported in the terms of streamlines, isotherms, wall temperature, and the velocity profiles in the cavity for a Richardson number of 0.1 and a Reynolds number equal to 100 and 1000. Their results showed that the maximum temperature values decrease as Reynolds number and Richardson number increase. The effect of the ratio between the channel and cavity heights is found to play a significant role on streamline and isotherm patterns for different heating configurations. The temperature distribution of an optical fiber traversing through a chemical vapor deposition reactor was obtained numerically by Iwanik and Chiu (2003). They indicated that, draw speed significantly affects fiber temperature inside the reactor, with temperature changed over 50% observed under the conditions studied.

Dianat *et al.* (2006) studied the highly turbulence flow inside gas–turbine combustors. In their study, they used the large eddy simulation (LES) of scalar mixing in a coaxial confined jet. Active control of turbulent separated flows over slanted surfaces was the objective of the study of Brunn and Nitsche (2006). They used the simple half diffuser configuration to demonstrate the receptivity of actuator perturbations in a quasi- two dimensional separated shear layer in terms of frequency spectra of velocity fluctuations measured.

An experimental study of pressure and velocity fields arising during normal injection of a radial slot into ducted flow is carried out by Terekhov and Mshvidobadze (2005). Their results showed that negative static pressure, whose value as it was expected increases with rise in the flow rate of the fan jet. Palm *et al.* (2006) studied experimentally and numerically the inflow conditions for a gas turbine swirl combustor. They indicated in their results that the axial velocity becomes increasingly asymmetric with the increase of swirl intensity. The velocity increases from the inside to outside of the annular flow corresponding to an intensified radial movement towards the outer wall due to imposed swirl.

The effect of velocity ratio on the turbulent mixing of confined co-axial jets was examined by Ahmed and Sharma (2000). Mean velocity, streamwise and turbulence intensity distributions at different streamwise locations were obtained using laser Doppler velocimeter (LDV) for different values of velocity ratios. Their results indicated that mixing process in confined jets depends strongly not only on the velocity ratio, but also on the interaction between the boundary layer, mixing layer and the main flow, particularly when the area ratio is small. The experimental study of buoyancy opposed wall jet flow was carried out by He *et al.* (2002). They measured the local velocity, turbulence intensities and temperature using Laser Doppler anemometry (LDA) and Thermocouples, in the flow field produced by a buoyancy-opposed wall jet discharging into a slowly moving counter- current stream in a vertical section of plane geometry. Their results showed that as the Richardson number is increased, the influence of buoyancy opposing the flow had the effect on the downward penetration of the jet

and its lateral spread. The turbulent impinging twin–jet flow was studied experimentally and numerically by Abdel-Fattah (2007). His results showed that the sub atmospheric region occurs on the impingement plate. It increases strongly by increasing Reynolds number and decreases as the jet angle and/or a nozzle to plate spacing increases. The spreading of jet decreases by increasing nozzle to plate spacing. The intensity of re-circulation zone between two jets decreases by increasing nozzle to plate spacing and jet angle. The increase of turbulence kinetic energy occurs within high gradient velocity.

The flow and thermal fields in a turbulent jet, impinging on a flat plate at an angle of incidence, has been studied numerically by Abdel-Fattah and Abd El-Baky (2009). The plate has a constant heat flux that transfers to the jet fluid and causes a temperature gradient in fluid. Computations were carried out with k-ε and v'^2 -f turbulence models. The flow characteristics were studied by changing plate inclination as ($0^0 \leq \theta \leq 45^0$), the distance between the nozzle exit and plate within $2 \leq H/b \leq 12$, and the Reynolds number in the range $2500 \leq Re \leq 12000$. Their results showed that the location of the maximum heat transfer was affected by the angle of inclination. The location of the maximum heat transfer shifts towards the up hill side of the plate by increasing the inclination angle. The value of the maximum Nusselt number increases with increasing nozzle to plate spacing. The pressure coefficient increases as the distance between the nozzle and the plate decreases.

The present paper concerns an experimental and numerical study for steady and turbulent flow in sudden enlargement with injection flow. The pressure recovery coefficient and the heat transfer characteristics are investigated by changing the injection flow angle and injection Reynolds number. Also, numerically, the velocity vector fields, velocities, turbulent kinetic energy and temperature contours at different injection flow rate and constant injection flow angle ($\theta = 0^o$) are presented in this work.

2. EXPERIMENTAL SETUP AND MEASURING METHODS

To carry out the experimental work, apparatus shown in Fig.1a is designed. The test rig consists of two centrifugal pumps, one for main flow and other for injected flow rate, pipeline connection, test section, injection system, supply tank and measuring devices (U-tube differential manometers and thermocouples). The test section is a circular sudden enlargement with 9 area ratios, made of commercial steel pipe with inlet nominal diameter 25.4 mm (1″) and outlet nominal diameter 76.2 mm (3″) and length 150 cm. 23 pressure taps of diameter (1 mm) and 12 thermocouples are distributed along the test section for static pressure and temperature measurement, respectively.

The injection system shown in (Figs. 1b and 1c) contains the chamber which provides the rectangular slots with different angles to inject hot water. The dimensions of rectangular slot jet are 15 mm x 2 mm. The required operating flow rate is adjusted using the injected flow pump and control valves. The volume flow rate for main and injection flow rates are measured by the orifice meter which is previously calibrated by collecting tank method.

The static pressure distribution, wall temperature distribution and outlet temperatures are measured. The pressure recovery coefficient is calculated using following equation:

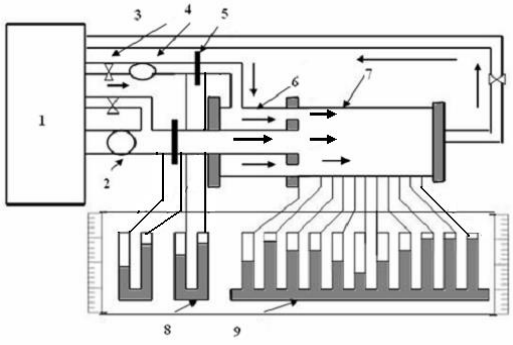

1. supply tank
2. main pump
3. control valve
4. injection Pump
5. Orifice meter
6. Injection system
7. Test section
8. U- tube differential manometer
9. Bank U -tube differential manometer

Fig.1a. Schematic layout of apparatus

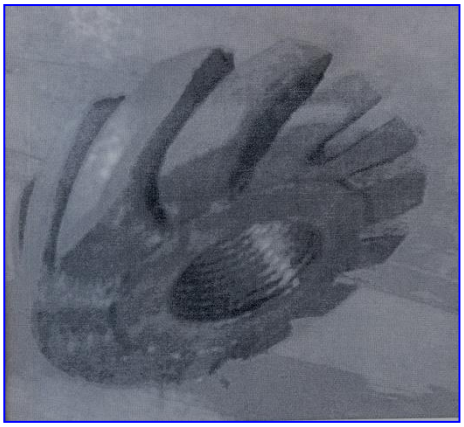

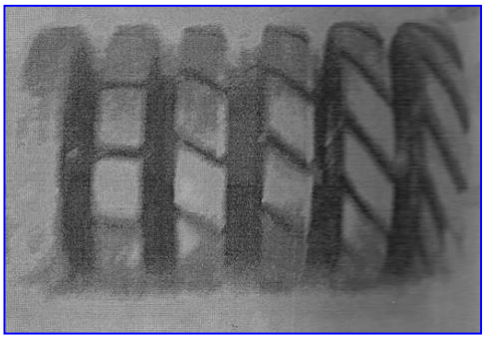

Fig. 1b. Flow guide for injection system

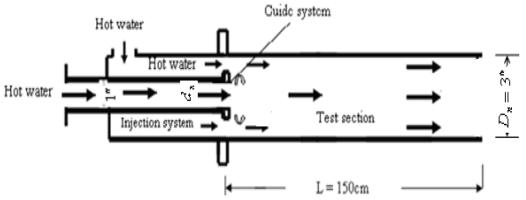

Fig.1c. The injection system

The static pressure distribution, wall temperature distribution and outlet temperatures are measured. The pressure recovery coefficient is calculated using the equation:

$$C_P = \frac{\bar{P} - \bar{P}_{in}}{0.5\rho U_m^2} \tag{1}$$

where U_m is the inlet mean velocity, $\bar{p}$ is the measured pressure and $\bar{p}_{in}$ is the measured pressure at inlet. The total net heat flow, q, can be expressed in terms of bulk-temperature difference by

$$\bar{q} = \dot{m}\, c_p\, (\bar{T}_{b_{in}} - \bar{T}_{b_{out}}) \tag{2}$$

where $\bar{T}_{b_{in}}$ is the entrance mean bulk temperature and $\bar{T}_{b_{out}}$ is the exit mean bulk temperature, c_p is the specific heat of fluid and $\dot{m}$ mass flow rate, calculated as:

$$\dot{m} = \rho\, A_f\, U_m \tag{3}$$

The net heat flow, $\bar{q}$, can be also expressed as:

$$\bar{q} = h_{av}\, A_S\, (\bar{T}_{b_{av}} - \bar{T}_{W_{av}}) \tag{4}$$

Then, the average heat transfer coefficient h_{av} is evaluated from the equation:

$$h_{av} = \frac{\bar{q}}{A_s (\bar{T}_{b_{av}} - \bar{T}_{W_{av}})} \tag{5}$$

where $\bar{T}_{b_{av}}$ is the fluid mean bulk temperature and $\bar{T}_{W_{av}}$ is the wall mean temperature. The following equations are used in calculating these temperatures.

$$\bar{T}_{b_{av}} = \frac{(\bar{T}_{b_{in}} + \bar{T}_{b_{out}})}{2} \tag{6}$$

$$\bar{T}_{w_{av}} = \sum_{i=1}^{i=N} \bar{T}_i / N \tag{7}$$

where $\bar{T}_i$ is the measured temperature and N is the number of measured values. Then, Nusselt number, Nu, is calculated, based on the hydraulic diameter, as follows:

$$Nu = \frac{h_{av} D}{k_c} \tag{8}$$

where k_c is the thermal conductivity

3. MATHEMATICAL MODELS

For solving the problem at zero inlet flow angle, the flow is considered two dimensional, steady, turbulent and incompressible fluid flow with no heat dissipation. The physical model used in this study is shown in Fig. 1a.

Based on the characteristics scales of d_m and U_m, the dimensionless variables are defined as follows.

$$r = \frac{\bar{r}}{d_m},\ z = \frac{\bar{z}}{d_m},\ k = \frac{\bar{k}}{U_m^2},\ u = \frac{\bar{u}}{U_m},\ v = \frac{\bar{v}}{U_m},\ p = \frac{\bar{p}}{0.5\rho U_m^2},\ T = \frac{(\bar{T} - \bar{T}_W)}{(\bar{T}_m - \bar{T}_W)},\ \varepsilon = \frac{\bar{\varepsilon}\, d_m}{U_m^3},\ \mu_t = \frac{\bar{\mu}_t}{\mu},\ \rho = \frac{\bar{\rho}}{\rho_i},\ Nu = \frac{h_{av} d_m}{k_c}$$

Here the over bar represents the dimensional quantities. According to the above assumptions and dimensionless variables, the dimensionless governing equations are expressed as the follows:

Continuity equation

$$\frac{1}{r}\left(\frac{\partial ru}{\partial z} + \frac{\partial rv}{\partial r}\right) = 0 \tag{9}$$

Axial momentum equation

$$u\frac{\partial u}{\partial z} + v\frac{\partial u}{\partial r} = -\frac{\partial p}{\partial z} + \frac{\partial}{\partial z}\left[\left(\frac{1}{\mathrm{Re}} + \frac{1}{\mathrm{Re}_t}\right)\frac{\partial u}{\partial z}\right] + \frac{1}{r}\frac{\partial}{\partial r}\left[r\left(\frac{1}{\mathrm{Re}} + \frac{1}{\mathrm{Re}_t}\right)\frac{\partial u}{\partial r}\right] + \frac{\partial}{\partial z}\left(\frac{1}{\mathrm{Re}_t}\frac{\partial u}{\partial z}\right) + \frac{1}{r}\frac{\partial}{\partial r}\left(\frac{r}{\mathrm{Re}_t}\frac{\partial v}{\partial z}\right) \tag{3}$$

Radial momentum equation:

$$v\frac{\partial u}{\partial z} + v\frac{\partial v}{\partial r} = -\frac{\partial p}{\partial r} + \frac{\partial}{\partial z}\left[\left(\frac{1}{\mathrm{Re}} + \frac{1}{\mathrm{Re}_t}\right)\frac{\partial v}{\partial z}\right] + \frac{1}{r}\frac{\partial}{\partial r}\left[r\left(\frac{1}{\mathrm{Re}} + \frac{1}{\mathrm{Re}_t}\right)\frac{\partial v}{\partial r}\right] + \frac{\partial}{\partial z}\left(\frac{1}{\mathrm{Re}_t}\frac{\partial v}{\partial z}\right) + \frac{1}{r}\frac{\partial}{\partial r}\left(\frac{r}{\mathrm{Re}_t}\frac{\partial v}{\partial r}\right) - \left(\frac{1}{\mathrm{Re}} + \frac{1}{\mathrm{Re}_t}\right)\frac{2v}{r^2} \tag{11}$$

Energy equation

$$u\frac{\partial T}{\partial z} + v\frac{\partial T}{\partial r} = \frac{\partial}{\partial z}\left[\left(\frac{1}{\mathrm{Re}\,\mathrm{Pr}} + \frac{1}{\mathrm{Re}_t\,\mathrm{Pr}_t}\right)\frac{\partial T}{\partial z}\right] + \frac{1}{r}\frac{\partial}{\partial r}\left[r\left(\frac{1}{\mathrm{Re}\,\mathrm{Pr}} + \frac{1}{\mathrm{Re}_t\,\mathrm{Pr}_t}\right)\frac{\partial T}{\partial r}\right] \tag{12}$$

The dimensionless equations for standard k- ε model are written as:

$$u\frac{\partial k}{\partial z} + v\frac{\partial k}{\partial r} = \frac{\partial}{\partial z}\left[\left(\frac{1}{\mathrm{Re}} + \frac{1}{\sigma_k\,\mathrm{Re}_t}\right)\frac{\partial k}{\partial z}\right] + \frac{1}{r}\frac{\partial}{\partial r}\left[r\left(\frac{1}{\mathrm{Re}} + \frac{1}{\sigma_k\,\mathrm{Re}_t}\right)\frac{\partial k}{\partial r}\right] + G - \varepsilon \tag{13}$$

$$u\frac{\partial \varepsilon}{\partial z} + v\frac{\partial \varepsilon}{\partial r} = \frac{\partial}{\partial z}\left[\left(\frac{1}{\mathrm{Re}} + \frac{1}{\sigma_\varepsilon\,\mathrm{Re}_t}\right)\frac{\partial \varepsilon}{\partial z}\right] + \frac{1}{r}\frac{\partial}{\partial r}\left[r\left(\frac{1}{\mathrm{Re}} + \frac{1}{\sigma_\varepsilon\,\mathrm{Re}_t}\right)\frac{\partial \varepsilon}{\partial r}\right] + c_1\frac{\varepsilon}{k}G - c_2\frac{\varepsilon^2}{k} \tag{14}$$

Here G is the rate of production of turbulent kinetic energy and is given by:

$$G = \frac{2S^2}{\mathrm{Re}_t} \tag{15}$$

and

$$S^2 = \frac{1}{2}\left[\left(\frac{\partial u}{\partial r}+\frac{\partial v}{\partial z}\right)^2 + 2\left(\frac{\partial v}{\partial r}\right)^2 + 2\left(\frac{v}{r}\right)^2 + 2\left(\frac{\partial u}{\partial z}\right)^2\right] \tag{16}$$

The values of the model constants are taken as reported by Leschziner and Rodi (1981), as follows:

c_1 =1.44 , c_2 = 1.92, c_μ =0.09, σ_k= 1 and σ_ε =1.3

Leschziner and Rodi (1981) incorporated the effects of stream line curvature on c_μ in the form.

$$c_\mu = Max\left\{0.025, \frac{0.09}{\left[1+0.57\frac{k^2}{\varepsilon^2}\left(\frac{\partial V_{tot}}{\partial n}+\frac{V_{tot}}{R_c}\right)\frac{V_{tot}}{R_c}\right]}\right\} \tag{17}$$

The curvature radius is calculated from:

$$\frac{1}{R_c} = \frac{uv\left(\frac{\partial v}{\partial r}-\frac{\partial u}{\partial z}\right)+u^2\frac{\partial v}{\partial z}-v^2\frac{\partial u}{\partial r}}{\left(u^2+v^2\right)^{1.5}} \tag{18}$$

The dimensionless form of dissipation equation for renormalization group model by Forliti and Strykowski (2005) is written as:

$$u\frac{\partial \varepsilon}{\partial z}+v\frac{\partial \varepsilon}{\partial r} = \frac{1}{r}\frac{\partial}{\partial r}\left[r\left(\frac{1}{\mathrm{Re}}+\frac{1}{\sigma_\varepsilon \mathrm{Re}_t}\right)\frac{\partial \varepsilon}{\partial r}\right]+\frac{\partial}{\partial z}\left[\left(\frac{1}{\mathrm{Re}}+\frac{1}{\sigma_\varepsilon \mathrm{Re}_t}\right)\frac{\partial \varepsilon}{\partial z}\right]+\frac{\varepsilon}{k}\left(c_1-\frac{\eta\left(1-\frac{\eta}{\eta_0}\right)}{1+\beta\eta^3}\right)G-c_2\frac{\varepsilon^2}{k} \tag{19}$$

where $\eta = \frac{k}{\varepsilon}\sqrt{2S^2}$

The values of the model constants are taken as:

$$c_\mu = 0.085,\ c_1 = 1.44,\ c_2 = 1.68,\ \sigma_k = 0.719,$$
$$\sigma_\varepsilon = 0.719,\ \eta_0 = 4.38\ and\ \beta = 0.012$$

Here the dimensionless eddy viscosity μ_t is given by the relation

$$\mu_t = c_\mu R_e \frac{\rho k^2}{\varepsilon}$$

The computational domain boundaries are shown in Fig. 2. The boundary conditions for the above set of governing equations are as follows:

a) Inlet Boundary

- At (a-b) and (e-f), the uniform velocity profiles and temperature are given by: $v = v_J \sin\theta$, $u = u_J \cos\theta$ and $T = T_j$
- At (c-d), the uniform velocity profiles and turbulent kinetic energy dissipation rate are i.e., u = 1, v = 0 , T =1, k = 0.01 and $\varepsilon = \frac{c_\mu k^{1.5}}{0.1}$

b) Wall Boundary

- At (b-c, d-e, f-g and h-a), the no slip boundary condition is imposed, and the wall function suggested by Launder and Spalding (1974) is used: $u = v = 0\ and\ T = 0$.

c) Exit Boundary

- At (g-h), a zero gradient condition is used for the outlet boundary. Although this boundary condition is strictly valid only when flow is fully developed, it is also permissible for sufficient downstream from the region of interest, i.e,

$\frac{\partial \phi}{\partial z} = 0\ and$ ϕ is one of the variables $u, v, T, k\ and\ \varepsilon$

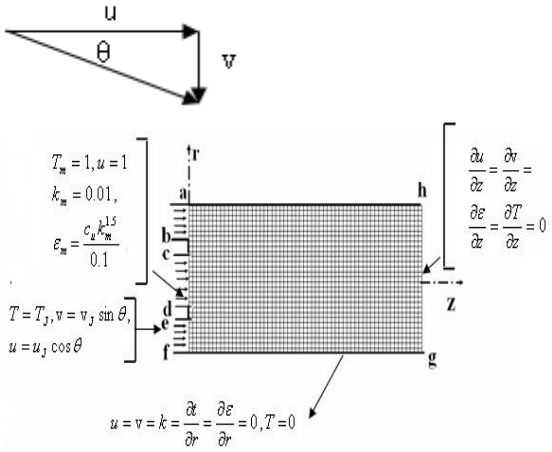

Fig. 2. Computational domain

4. SOLUTION PROCEDURE

The mathematical models described above consist of a set of differential equations subject to appropriate boundary conditions. To provide the algebraic form of the governing equations, a fully staggered grid system was adopted for the velocity components and the scalar variables. These equations were discretized using a control volume finite difference method (CVFDM). The numerical solution in the present work is accomplished using Semi- Implicit Method for Pressure Linked Equation (SIMPLE) utilized by Patankar (1980). The velocity components u is calculated at the east and west faces of the main control volumes from the solution of the axial momentum equation. Similarly, the velocity component v at the north and south faces is calculated. When the pressure correction equation is solved, the velocity and the pressure fields are corrected. To complete iteration, the energy equation and the turbulent kinetic energy and energy dissipation rate are solved successively. The discretized equations were solved by the line by line procedure, which is a combination of Gauss- Seidel and tridiagonal matrix algorithm in the stream wise direction. The tridiagonal matrix algorithm (TDMA) was used to solve a set of discretized equation in the cross–equations in the cross–stream direction. Relaxation factors were used to promote smooth convergence of the discretized equations. The relaxation factors were 0.5, 0.5, 0.5, 0.8, 0.85 and 0.85 for u, v, p', T, k and ε, respectively. The

turbulent viscosity was under relaxed at a value of 0.85. The converged criterion in this study was based on the successive changes in variables. All field variables were monitored, and the following condition was used to declare convergence:

$$MAX\left|\frac{\phi_{i,j}^{n}-\phi_{i,j}^{n-1}}{\phi_{i,j}^{n}}\right| \le 10^{-4} \qquad (20)$$

In addition, the ratio of the difference between the inlet mass flow rate and the outlet mass flow rate to the inlet mass flow rate was also examined. Convergence was declared if the relative mass imbalance less than 10^{-3} and Eq. (20) were satisfied simultaneously. After the convergence the flow at this time step**,** the entire variables are taken as the initial condition for the new time step. To verify the algorithm, numerical tests were performed to ensure that the solution was grid independent. The grid points are distributed uniformly over the computational domain. A 155 x 41 grid points were placed in the computational domain in Fig. 2. Results at a grid independent study are shown in Fig. 3a. The effect of the turbulence models on the pressure recovery coefficient is shown in Fig. 3b.

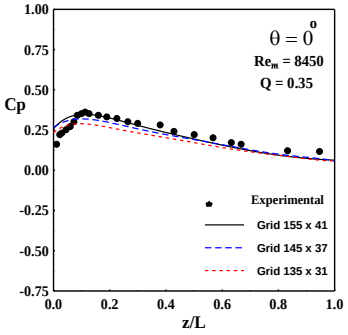

Fig. 3a. Effect of grid refinement on the pressure recovery coefficient

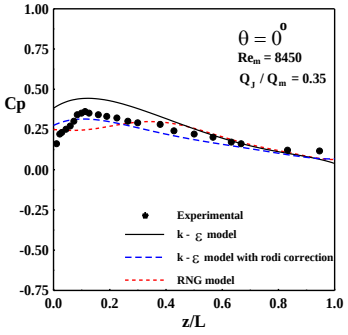

Fig. 3b. Effect of turbulence model on the pressure recovery coefficient

5. RESULTS AND DISCUSSION

5.1 Velocities Contours

A representative selection of axial velocity contours using the numerical results ($\bar{u}/U_m$) for different values of flow injection ratio at injection angle ($\theta = 0^o$) are shown in Fig. 4. From Fig. 4a, for the flow without injection flow, it can be seen that the velocity concentrates at chamber center and decreases in the radial direction. It also decays in down stream direction. This is because the main flow becomes more spreader as it comes far from inlet section. The main flow becomes more concentrated by injecting flow in recirculation zone. This flow concentration extends in downstream direction by increasing the injection flow rate (Figs. 4a to 4d). For the same injection flow rate, as the main flow rate decreases, the flow becomes more concentrated at chamber center and the recirculation zone between the main flow and the injection flow becomes clearer (Fig. 4e).

The profiles of the radial velocity contours ($\bar{v}/U_m$) are shown in Fig. 5. From this figure, it can be seen that the intensity of secondary flow in recirculation region decreases by increasing the injection flow rate. This is due to the injection of the axial flow in the recirculation zone behind the step at the inlet. The recirculation zone decreases at higher value of injection flow rate for constant value of injection flow rate and small value of the main flow (Fig. 5e)

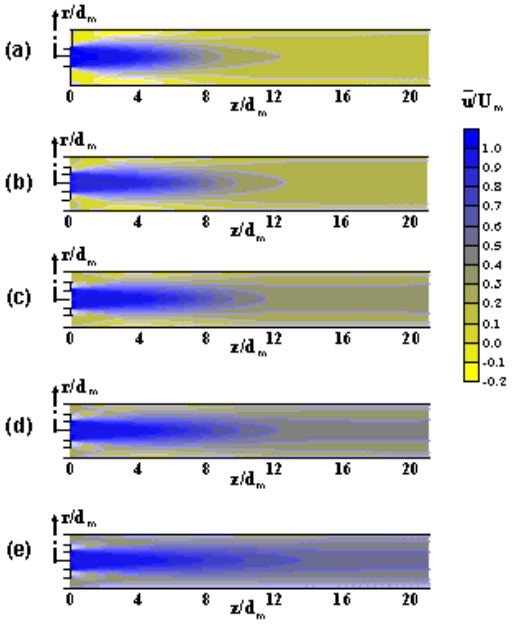

No	Q	Re_m
a	0	8450
b	0.17	8450
c	0.25	8450
d	0.35	8450
e	0.43	5895

Fig. 4. Axial velocity contours ($\bar{u}/U_m$) at injection flow angle ($\theta = 0^o$) using the k-ε model with Leschziner and Rodi correction for different injection ratio, Q, and Re_m.

5.2 Turbulent Kinetic Energy Contours

The turbulent kinetic energy contours ($\bar{k}/U_m^2$) obtained numerically for Re_m = 8450 using the k-ε model with Leschziner and Rodi correction (1981), are shown in Fig. 6. From Fig. 6a, corresponding to the case for the flow in a sudden enlargement without

injection, it can be noticed that an increase in turbulent kinetic energy

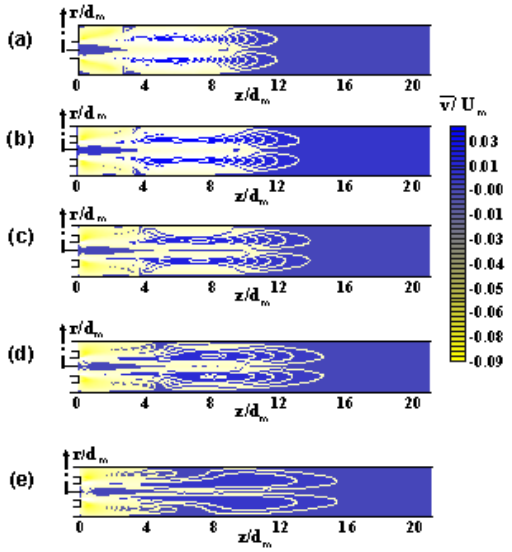

No	Q	Re_m
a	0	8450
b	0.17	8450
c	0.25	8450
d	0.35	8450
e	0.43	5895

Fig.5. Radial velocity contours ($\bar{v}/U_m$) at injection flow angle (θ = 0º) using the k-ε model with Leschziner and Rodi correction (1981) for different injection ratio, Q, and Re_m.

happens within regions between the recirculation zones and main zones. This is due to the big velocity gradient in these regions. This turbulent kinetic energy decays by injecting flow in the recirculation zone.

This is due to small velocity gradient in those regions (Figs 6b and 6d). As the injection ratio increases at constant injection angle (θ = 0º) and constant main flow rate, the turbulent kinetic energy decreases but the length of higher turbulent kinetic energy increases. This is due to the increase of the size of mixing zone between the main flow and injection zone. The increment of turbulent kinetic energy in that regions decreases by increasing the injection flow rate. This is due to the decrease of the velocity gradient between the injection flow and the main flow leading consequently to a reduction of the flow turbulence. The turbulence of the flow is seen to decrease with the main flow rate for the case of constant injection flow rate (Fig. 6e).

5.3 Temperature Contours

A representative selection of the temperature contours $\frac{(\bar{T}-\bar{T}_W)}{(\bar{T}_m-\bar{T}_W)}$ for Re_m = 8450, using the k-ε model with Leschziner and Rodi correction (1981) is shown in Fig. 7. From this figure, in case without injection flow in recirculation zone of sudden enlargement, it is seen that flow temperature is high at the initial zone of the pipe and decreases at down stream direction. Also, it can be seen that the flow temperature in the recirculation zone is smaller than the flow temperature at the pipe center.

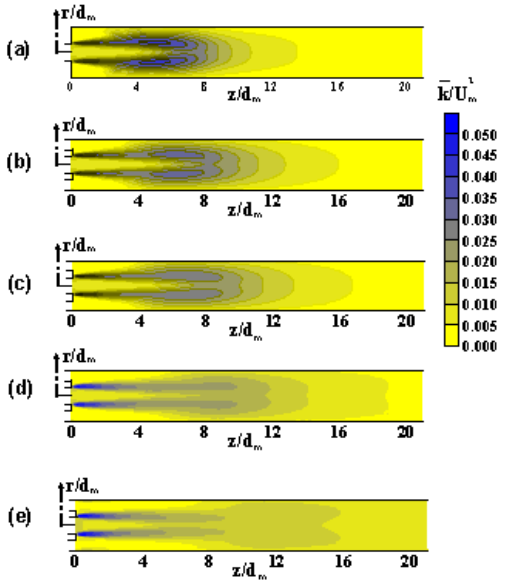

No	Q	Re_m
a	0	8450
b	0.17	8450
c	0.25	8450
d	0.35	8450
e	0.43	5895

Fig. 6. Turbulent kinetic energy contours ($\bar{k}/U_m^2$) at injection flow angle (θ = 0º) using the k-ε model with Leschziner and Rodi correction (1981) for different injection ratio, Q, and Re_m.

This is due to the secondary flow and heat transfer increase which lead to the heat rejection increase and consequently to a decrease of the temperature with downstream direction, (Fig. 7a). By injecting hot fluid in recirculation zone at same temperature of main flow, the intensity of secondary flow decreases and the flow temperature in recirculation zones is higher than the flow temperature for the case without injection. This is due to the decrease of the flow turbulence in this zone then the heat rejection decreases consequently the temperature increases in that region. As the injection flow ratio increases at constant injection flow angle (θ = 0º), the flow momentum increases then the length of the higher temperature region increases (Figs. 7b to 7d). In case of constant injection flow rate and low main flow rate, the length of higher temperature region increases. This is due to the secondary flow becomes very less consequently the heat transfer decrease then the temperature becomes bigger (Fig. 7e).

5.4 Effect of Reynolds Number on the Pressure Recovery Coefficient

Figures 8a to 8e show the pressure recovery coefficient ($\bar{P}-\bar{P}_{in}/0.5\rho U_m^2$) measured for different values of inlet flow angle as a function of axial distance (z/L), each figure for different values of injection ratio. From

these figures, in the case of sudden enlargement without injection flow ($Q = 0$), it is seen that, generally, the local pressure recovery decreases to reach a minimum value through the recirculation zone behind the step which causes increase of hydraulic losses. Then the pressure coefficient increases to maximum value at reattachment point and starts to decrease again gradually in the downstream direction due to the friction effect. It is evident that in the case of no injection, a short region of favorable streamwise gradient exists after the step. In addition, it can be noticed that an increase of the injection ratio above zero value causes an increase of the pressure coefficient.

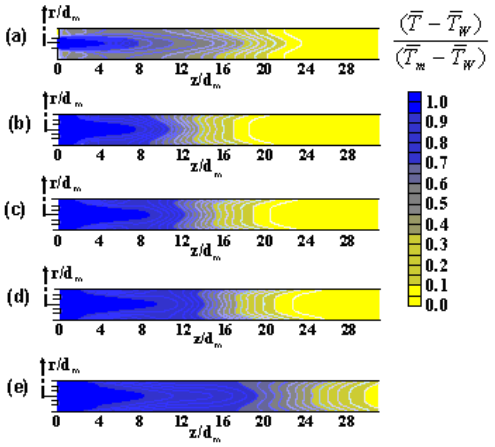

No	Q	Re_m
a	0	8450
b	0.17	8450
c	0.25	8450
d	0.35	8450
e	0.43	5895

Fig. 7. Flow temperature contours $(\bar{T} - \bar{T}_W)/(\bar{T}_m - \bar{T}_W)$ at injection flow angle (θ = 0º) using the k-ε model with Leschziner and Rodi correction (1981) for different injection ratio, Q, and Re_m.

Also it can be seen that, the pressure recovery coefficient increases by increasing the injection flow angle. This can be explained by an increase of the kinetic energy which affects of the pressure coefficient. Also, it is noticed that the peak of the pressure recovery decreases by increasing the injection flow ratio Q. In addition, Fig. 8a indicates the comparison between the experimental and numerical work using the k-ε model with correction of Leschziner and Rodi (1981) at inlet flow angle ($\theta = 0$º). The comparison gives a good agreement between the experimental and numerical results.

5.5 Effect of the Injection Flow Angle on the Pressure Recovery

Figure 9 shows the pressure Recovery coefficient ($\bar{P} - \bar{P}_{in} / 0.5\rho U_m^2$) as a function of axial distance (z/L) at different values of the injection flow angle (θ = 0º, 30º and 60º) and constant value of the injection ratio (Q = 0.35). The numerical values were calculated using the k-ε model with correction of Leschziner and Rodi (1981) at zero inlet flow angle. From this figure, it

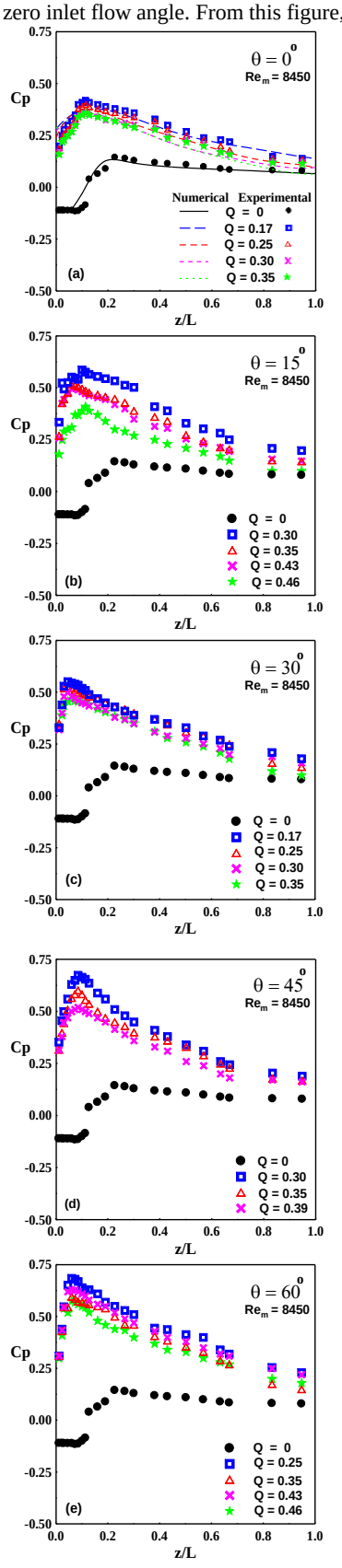

Fig. 8. Variation of the pressure recovery coefficient of different values of injection ratio ,Q, at injection flow angle (0^0, 15º, 30º, 45º and 60º) at Re_m = 8450.

can be seen that the pressure recovery coefficient before the reattachment point increases as the injection flow angle increases.

In fact, the increase of the injection flow angle leads to an increase of the radial component velocity, and consequently the kinetic energy which converts into pressure, increases. Also, the peak of the pressure coefficient moves award in the upstream direction with increasing injection flow angle. This is due to the decrease of the recirculation zones between the main flow and injection flow when the injection flow angle is increased and consequently the reattachment point shifts toward the upstream direction.

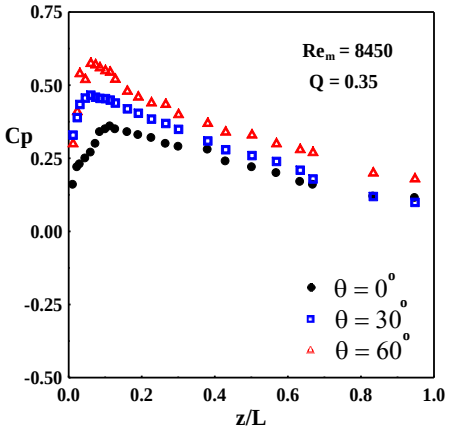

Fig. 9. Variation of pressure coefficient at different values of injection flow angle at Re_m = 8450 and Q = 0.35.

5.6. Average Heat Transfer

Overall Nusselt numbers along the sudden enlargement are presented in this section the main Reynolds number (Re_m), the injection Reynolds number (Re_j) and the injection flow angle. The numerical results are calculated using the k-ε model with correction of Leschziner and Rodi (1981).

Figure 10a represents the variations of the Nusselt number as function of the Reynolds number of the main flow in sudden enlargement (Re_m) without injection flow (Q = 0). From this figure, it can be seen that the Nusselt number increases as the Reynolds number of main flow increases. The effect of injection Reynolds number on Nusselt number at constant main Reynolds number (Re_m = 8450) is shown in Figs 10b and 10c. The results indicted that, generally, the values of Nusselt number increase, due to the increase of injection Reynolds number at all values of injection flow angle. The reason for this tendency may be due to the momentum increases as Reynolds number of injected flow increases causing an increase in the heat transfer coefficient. Although Nusselt number increases as Reynolds number of injected flow increases but this increase does not reach to the value of Nusselt number in case of the flow without injection with constant value of main flow. This is due to reduce the recirculation zones. Injecting hot flow in recirculation zones causes to decreases or finishes the intensity of secondary flow then the heat transfer decreases.

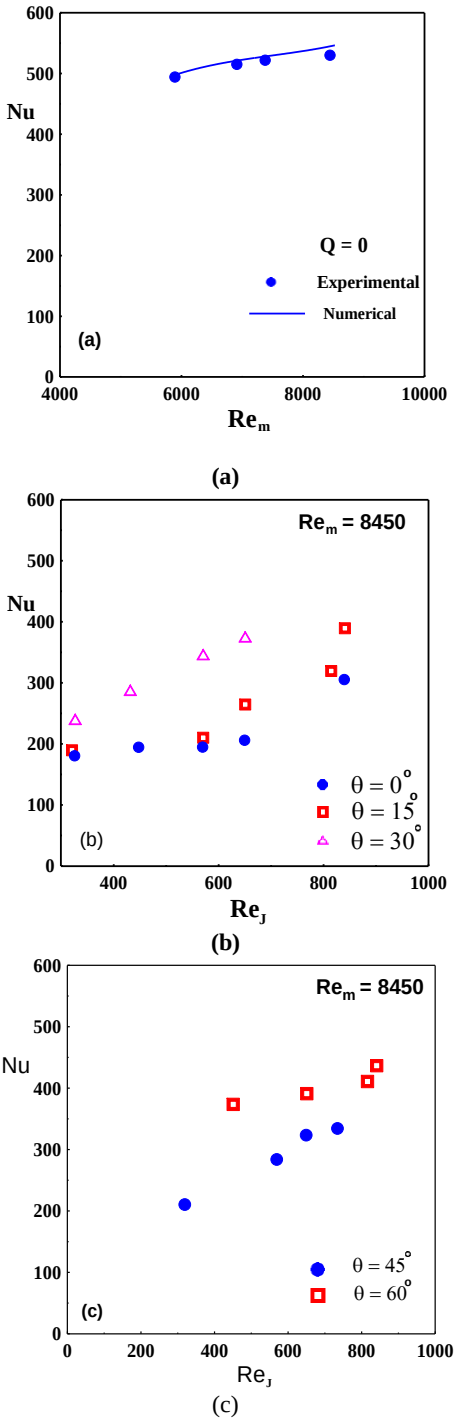

Fig.10. Variation of average Nusselt number with Reynolds number for injection flow angle (a) without injection (Q = 0) using the k- ε model with Leschziner and Rodi correction (1981) (b) θ = 0º, = 15º and 30º and (c) θ = 45º and 60º

6. CONCLUSIONS

The behavior of the fluid flow of steady incompressible turbulent from the wall injection into main flow in sudden enlargement was carried out experimentally and numerically. The effect of injection ratio, Reynolds number and the injection flow angle on the pressure recovery coefficient, the heat transfer characteristics are

studied experimentally, and the velocity vector, velocities, turbulent kinetic energy and temperature contours are obtained numerically. The major conclusions of this research could be summarized as follows:

- The axial velocity concentrates in the medial chamber and the maximum value of this velocity extends in down stream direction by increasing the injection flow rate.
- The turbulent kinetic energy increases within region between the recirculation zones and main zone and it decays by injecting flow in the recirculation zone.
- The length of zone for higher value of flow temperature decreases by injecting flow in the recirculation zone, and that length increases as the injection flow rate increases.
- The pressure recovery coefficient increases by increasing injection ratio and also its peak value, at the reattachment point increases as injection flow ratio increases.
- As the injection flow angle increases, the pressure recovery increases and its maximum value at the reattachment point shifts in upstream direction by increasing the injection flow angle.
- The value of the Nusslet number increases as injection Reynolds number increases, also it increases as the injection flow angle increases.
- For all cases of injection in recirculation zone of sudden enlargement, the heat transfer is less than that corresponding to the flow without injection.
- The comparison between the numerical results and the experimental measurements in terms of the average Nussel number gives good agreement using the k-ε model with correction of Leschziner and Rodi (1981).

REFERENCES

Abdel-Fattah, A. (2007). Numerical and experimental study of turbulent impinging twin–jet flow. *Experimental Thermal and Fluid Science* 31,1061-1072.

Abdel-Fattah, A. and Abd El-Baky (2009). Numerical investigation of impinging two dimensional jet on an inclined flat plate. *International Journal of Fluid Mechanics Research* 36(5), 391-413.

Ahmed, M.R., and S.D. Sharma (2000). Effect of velocity ratio on the turbulent mixing of confined, co –axial jets. *Experimental Thermal and Fluid Science* 22, 19-33.

Brunn, A. and W. Nitsche (2006). Active of turbulent separated flows over slated surfaces. *International Journal of Heat and Fluid Flow* 27, 748-755.

Dianat, M., Z. Yang, D. Jiang and J.J. McGuirk (2006). Large eddy simulation of scalar mixing in a coaxial confined jet. *Flow Turbulence Combust*. 77, 205-227.

Forliti, D.J. and P.J. Strykowski (2005). Controlling turbulence in a rearward – facing step combustor using countercurrent shear. *Journal of Fluid Engineering* 127, 438-448.

He, S., Z. Xu and J.D. Jackson (2002). An experimental investigation of buoyancy- opposed wall jet flow. *International Journal of Heat and Fluid Flow* 23, 487-496.

Iwanik, P.O and W.K.S. Chiu (2003). Temperature distribution of an optical fiber traversing through a chemical vapor deposition reactor. *Numerical Heat Transfer Part A* 43, 221-237.

Kanna, P.R. and M.K. Das (2006).Heat transfer study of two –dimensional laminar incompressible wall jet over backward –facing step. *Numerical Heat Transfer Part A* 50, 165- 187.

Launder, B.E., D.B. Spalding (1974). The numerical computation of turbulent flow. *Comput. Methods Appl. Mech. Eng.* 3, 269-289.

Leschziner, M.A., W. Rodi (1981). Calculation of annular and twin parallel jets using various discretization schemes and turbulence- model variations. *ASME Fluids Eng.* 103.

Lindstedt, R.P., D.S. Luff and J.H. Whitelaw (2005). Velocity and strain –rate characteristics of opposed isothermal flows, Flow. *Turbulence and combustion* 74, 169-194.

Manca, O., S. Nardini, K. Khanafer and K. Vafai (2003). Effect of heated wall position on mixed convection in a channel with an open cavity. *Numerical Heat Transfer Part A* 43, 259-282.

Palm, R., S. Grundmann, M. Weismüller, S. Ŝarić, S. Jakirlić, and C. Tropea (2006). Experimental characterization and modeling of inflow conditions for a gas turbine swirl combustor. *International Journal of Heat and Fluid Flow* 27, 924-936.

Patankar, S.V. (1980). *Numerical Heat Transfer and Fluid Flow*. McGraw-Hill, New York.

Seo, E. and S. Parameswaran (2002). Numerical computations of steady and unsteady, separation buoyant flows- Part1: computations with the standard k-ε model. *Numerical Heat Transfer Part A* 42, 791- 809.

Terekhov, V.I., Yu, and M. Mshvidobadze (2005). Experimental investigation flow structure and hydraulic resistance of a cylindrical duct with injection a fan slot jet. *Experimental Thermal and Fluid Science* 29, 159-167.

Yilmaz, I. and H.F. Öztop (2006). Turbulence forced convection heat transfer over double forward facing step flow. *International Communication in Heat and Mass Transfer* 33, 508-517.